Application of the Varshni model and Raman spectroscopy for the analysis of shock effects in semiconductors

© E.Kh. Khamzin, S.A. Nefedov, D.N. Artemyev

Samara National Research University,
443086 Samara, Russia

E-mail: elkhan.k.khamzin@gmail.com

Received May 25, 2026
Revised July 6, 2026
Accepted July 21, 2026

The application of the Varshni model in combination with Raman spectroscopy to study changes in the electrical properties of semiconductor wafers under impact loading is considered using the example of *p*-type single-crystal silicon doped with boron (resistance $10\,\Omega \cdot$ cm). Raman spectroscopy serves as an efficient tool for monitoring crystal lattice modifications, providing an indirect estimation of variations in the band gap, dielectric permittivity, lattice parameter, and covalent bond length. A methodology for recording Raman spectra and interpreting experimental data within the Varshni model framework is described. Relationships established between vibrational frequencies and physical parameters of the material demonstrate band gap narrowing, an increase in dielectric permittivity, and an expansion of interatomic distances under shock-wave mechanical loading. The observed regularities highlight the potential of tuning semiconductor parameters for photonic, power, and sensor applications. Furthermore, the results confirm the effectiveness of combining Raman spectroscopy with the Varshni model for structural change analysis without relying on resource-intensive numerical simulations.

Keywords: Raman spectroscopy, Varshni model, solid semiconductors, shock-wave processing, band gap, dielectric constant, lattice parameter, structural changes.

DOI: 10.61011/SC.2026.05.63995.9931

1. Introduction

Modern semiconductor materials underpin a broad range of technologies, including photonics, power electronics, and sensor systems [1–3]. Structural changes induced by mechanical loading, particularly shock loading, are among the key factors affecting material properties. Studying these changes is important for understanding material degradation mechanisms and developing devices with improved reliability and functionality [4–8].

Raman spectroscopy (RS) is an established method for sensitive, nondestructive probing of microstructural changes in semiconductors, enabling assessment of lattice parameters, vibrational modes, and electronic properties [3,9–11]. However, quantitative analysis and interpretation of experimental data require models, such as the Varshni model [12–16], that relate spectral changes to mechanical strain and changes in functional material parameters [17–19].

Despite progress in understanding the effects of pressure and strain on semiconductors, a comprehensive analysis of shock loading that accounts for pressure gradients and the penetration depth of probe radiation and predicts the resulting electrical properties remains largely unresolved. Addressing this problem would improve predictions of material behavior under extreme conditions and help optimize properties for specific applications.

Here we adopt an established approach used in the micro- and nanomechanics of semiconductor structures, in which phonon frequency shifts in Raman spectra correlate directly with mechanical strain and stress in the crystal. This correlation has been experimentally confirmed for silicon and other materials in numerous studies and is widely used to map strain and stress in microstructures and microelectromechanical systems (MEMS) [20]. Theoretical models relating the strain tensor to the observed Raman shift for uniaxial and biaxial compressive stress in Si, accounting for crystallographic orientation, have been developed and verified experimentally [21].

We therefore consider it justified to use the measured Raman spectra to estimate shock-induced mechanical strain and subsequently determine changes in the structural and electronic parameters using an appropriate parametrization of the Varshni model. This assumption defines the objectives of the present study: analysis of shock effects in a semiconductor silicon wafer, identification of relationships between spectral characteristics and key physical material parameters, and discussion of the potential use of these results in developing new electronic devices.

2. Materials and methods

A silicon wafer sample with crystallographic orientation [100] (KDB-10) was subjected to controlled shock loading using a solid-state Nd:YAG laser with a wavelength of $\lambda = 532$ nm, an incident energy of 0.310 J, and a pulse duration of 10 ns. A schematic of the shock-wave generation setup and a photograph of the sample are shown in Figure 1, *a, b*. The radiation passed through air, acrylic glass, and a water layer, then was partially reflected

by the textured silicon surface. Accounting for energy losses and reflectance, an energy of 0.215 J reached the interaction region, 2 mm in diameter. Estimates of the shock parameters indicated that this pulse energy produced a shock wave with a velocity of ~ 8575 m/s. This is consistent with the elastic precursor velocity in silicon ($\sim 8.1-8.5$ km/s for [100]) [22], indicating the absence of plastic flow. According to Ref. [23], no phase transitions or amorphization occur in silicon up to ~ 10 GPa, and structural changes are limited to the elastic lattice response. These findings support the applicability of the approach described below: using RS to assess exclusively elastic (quasilinear) crystal strain.

3. Raman spectroscopy (RS)

Raman measurements were performed without ambient illumination using a PHOTON-BIO microscope with 532 nm laser excitation and 20× magnification (laser power 15 mW). Spectra were recorded in a darkened room to eliminate contributions from stray light. For each spectrum, a background signal was measured with the laser off and subsequently subtracted. All Raman measurements were performed at room temperature, allowing the thermal contribution to be excluded and the mechanical origin of the changes to be isolated.

Mechanical loading induces crystal strain, which can change interatomic distances and lattice symmetry. This strain can be quantitatively related to optical phonon frequency shifts in Raman spectra through a piezo-Raman approach that links stress to the observed frequency shift. For a diagonal stress tensor, particularly under hydrostatic stress, where its principal components are equal ($\sigma_{xx} = \sigma_{yy} = \sigma_{zz}$) and off-diagonal components vanish, the relation between the frequency shift $\Delta\omega$ and equivalent pressure P can be written in scalar form: $\Delta\omega = KP$, where K is a calibration coefficient (e.g., $\sim 5.2\,\mathrm{cm}^{-1}$/GPa for Si according to Ref. [24]).

Strain ε changes the lattice parameter a and interatomic distance d, described to first order by $\Delta a/a \approx -PE$, where E is Young's modulus. The strain-induced band gap correction ΔE_g is described by deformation potential theory under the assumption of an axisymmetric stress state:

$$\Delta E_g = a_v(\varepsilon_{xx} + \varepsilon_{yy} + \varepsilon_{zz}) + b\left(\varepsilon_{zz} - \frac{\varepsilon_{xx} - \varepsilon_{yy}}{2}\right), \quad (1)$$

where a_v and b are the material's deformation potentials (values for Si are available in the specialized literature [25]).

Thus, combining the measured Raman shift $\Delta\omega$, calculated stress or strain, and known material parameters enables estimation of changes in the lattice parameter a, covalent bond length d, band gap E_g, and, if needed, dielectric constant ε, since phonon vibrations are related to the electron cloud distribution and lattice polarizability. This approach directly applies established deformation potential theory and Raman microspectroscopy to quantitatively interpret structural and electronic changes under mechanical loading.

4. Varshni model

The spectral data were interpreted using the Varshni model [26], which describes the temperature dependence of the band gap:

$$E_g(T) = E_g(0) - \frac{aT^2}{T+\beta}, \quad (2)$$

where $E_g(0)$, α, and β are empirical parameters fitted to experimental data. The physical basis of the model is renormalization of the electronic band structure due to electron–phonon coupling. Changes in the crystal phonon spectrum, regardless of their origin, shift the valence and conduction band edges in opposite directions, thereby changing the band gap. Here the changes in phonon properties are caused by mechanical strain of the crystal lattice induced by shock loading, rather than temperature. Since strain changes interatomic distances, lattice symmetry, and vibrational frequencies, the Varshni model is used here as an effective parametric tool for describing the influence of strain-induced changes in the phonon spectrum on the electronic properties of the semiconductor within its elastic response regime. Thus, the Varshni model can be related to parameters affecting the phonon structure. We propose to establish this relation without introducing additional empirical coefficients through pseudothermodynamic variables, such as k, $T_{\text{eff}} = k \cdot (\omega_0 - \omega)$. Instead, the relation is constructed through the vibrational frequency associated with shock-wave pressure:

$$P(\omega) = \frac{\omega - \omega_0}{\partial\omega/\partial P}, \quad (3)$$

where $\partial\omega/\partial P \approx 5.2\,\mathrm{cm}^{-1}$/GPa is the coefficient cited above. The expression for E_g then becomes

$$E_g(P) = E_{g0} + \frac{\partial E_g}{\partial P} \cdot P. \quad (4)$$

Since electronic structure depends directly on interatomic distances and lattice symmetry, mechanical strain induced during shock-wave exposure changes both the structural and electrical properties of the semiconductor, particularly the lattice parameter, covalent bond length, band gap, and dielectric constant. After the equivalent residual pressure was inferred from the silicon LO phonon shift using the calibration coefficient $\partial\omega/\partial P$, the lattice parameter a, covalent bond length d, and permittivity ε were estimated using linearized equations of state:

$$a(P) = a_0 + \left(\frac{\partial a}{\partial P}\right)P,$$

$$d(P) = d_0 + \left(\frac{\partial d}{\partial P}\right)P,$$

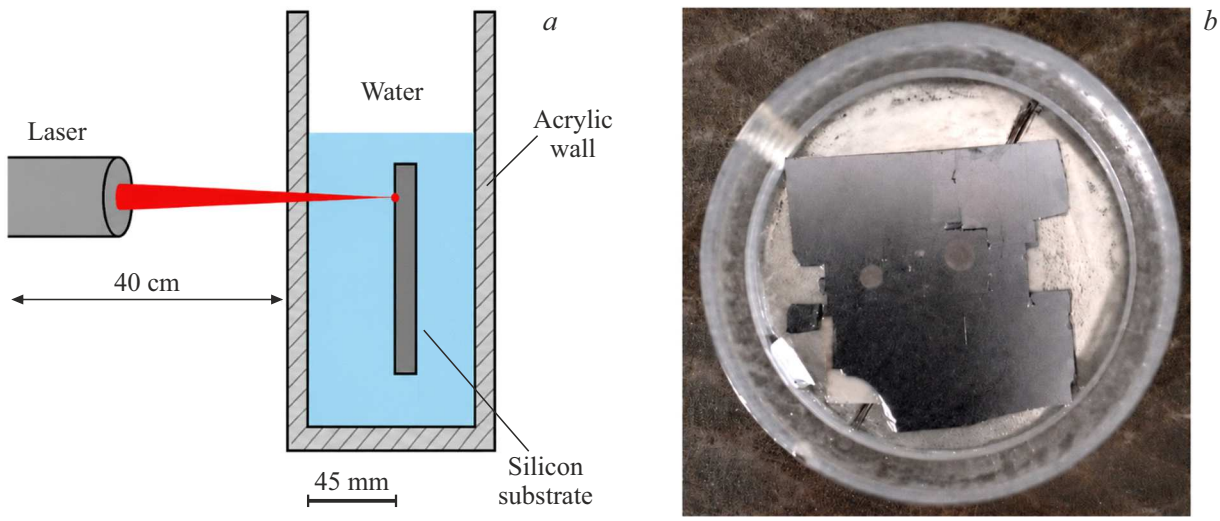


Figure 1. *a* — schematic of the shock-wave generation setup; *b* — photograph of the silicon wafer.

$$\varepsilon(P) = \varepsilon_0 + \left(\frac{\partial \varepsilon}{\partial P}\right)P, \tag{5}$$

where a_0, d_0, and ε_0 are the values in the unloaded state. The derivatives $\partial a/\partial P$, $\partial d/\partial P$, and $\partial \varepsilon/\partial P$ are determined from the elastic moduli, compressibilities, and known silicon deformation potentials widely used in the theory of strained semiconductors. For a cubic lattice, the relative lattice parameter change is related to pressure through the bulk modulus K by $\frac{\Delta a}{a} = -\frac{P}{3K}$. The Si–Si covalent bond length was obtained geometrically from the lattice parameter as $d = (\sqrt{3}/4)a$. The permittivity change was estimated using a linear dependence on volumetric strain:

$$\frac{\Delta \varepsilon}{\varepsilon} = -\gamma_\varepsilon \frac{\Delta V}{V}, \tag{6}$$

where γ_ε is a dimensionless coefficient characterizing the sensitivity of electronic polarizability to volume changes and is of order unity for silicon [27].

The proposed approach is applicable only in the elastic strain regime, where shock loading does not cause phase transformations, amorphization, or significant material heating. Within the shock-wave parameter range considered, the optical phonon frequency and associated band structure parameters vary linearly. This justifies using the Raman shift to infer the equivalent pressure and subsequently analyze the electronic properties of silicon.

5. Results and discussion

Figure 2 shows Raman spectra of KDB-10 single-crystal silicon before and after shock loading. The most significant observed effect is a shift of the principal Si–Si phonon mode (the bond vibration at $\approx 520.7\,\mathrm{cm}^{-1}$ in the initial state [28]) toward lower frequencies on approaching the shock epicenter. The spectral linewidth (FWHM) increases at the same time, indicating a higher defect concentration

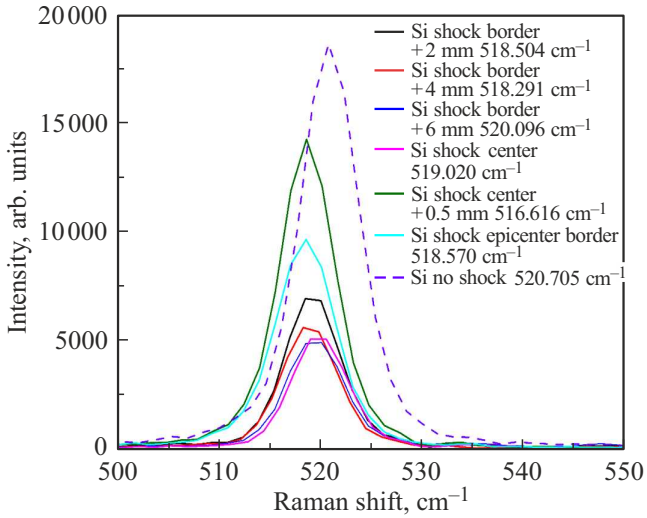


Figure 2. Raman spectra of the sample studied.

and disruption of long-range lattice order due to local mechanical stress [29,30].

The changes were interpreted quantitatively using the modified Varshni equation (3), which relates the band structure parameters to shock-wave pressure through the acoustic lattice response, rather than to temperature. The experimentally observed frequency shift yielded $E_g(P)$, $\varepsilon(P)$, $a(P)$, and $d(P)$ dependences, shown in Figure 3.

The equations of state are assumed to remain linear over the pressure range considered, and crystalline order is assumed to be retained in the spectrally probed region. Above the plasticity threshold, the relation between the phonon peak position and band structure changes, making the model inapplicable without accounting for nonlinear processes.

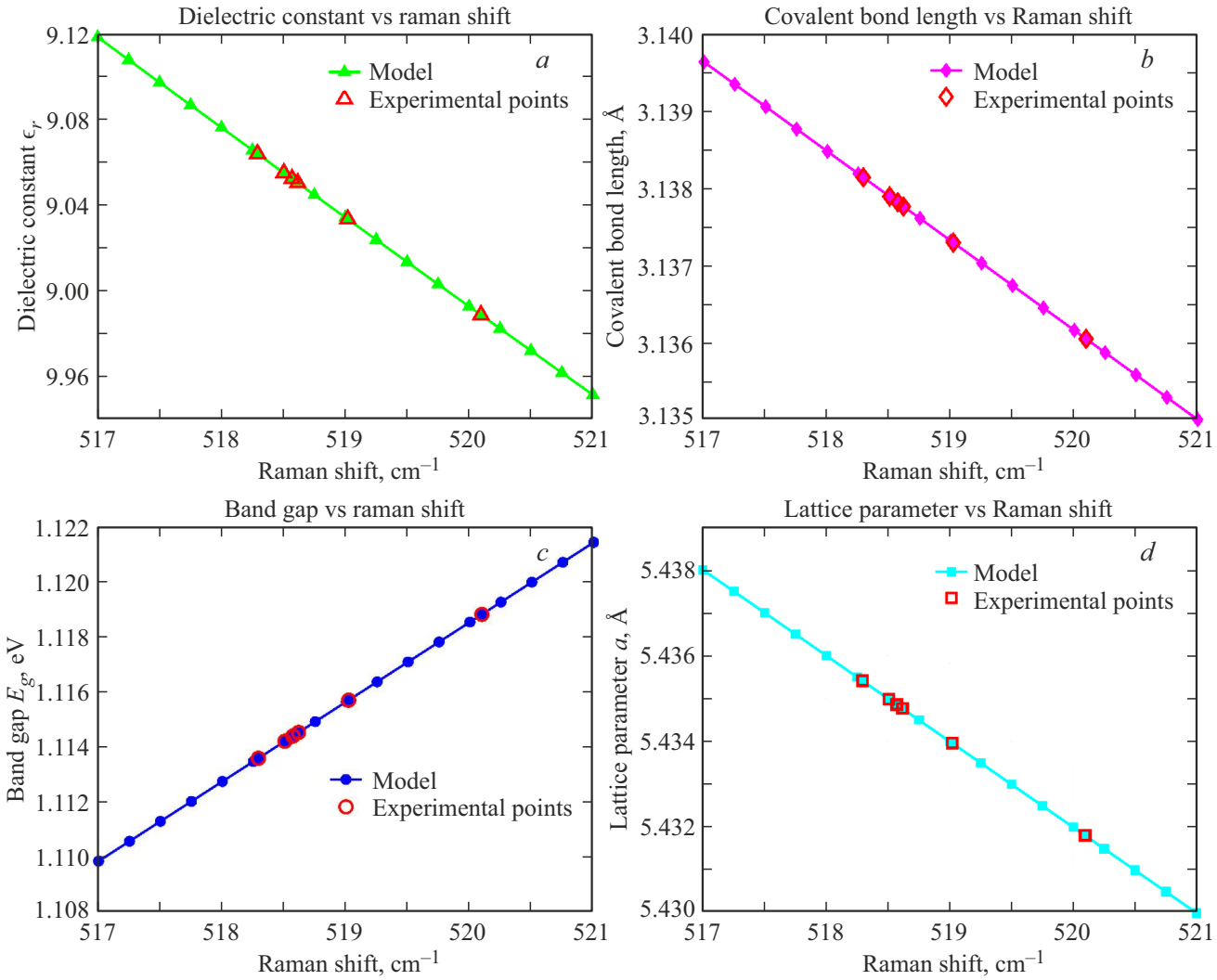


Figure 3. Band structure parameters of a shock-treated silicon wafer as functions of the observed Raman shift: a — dielectric constant $\varepsilon(P)$; b — covalent bond length $d(P)$; c — band gap $E_g(P)$; d — lattice parameter $a(P)$.

Shock loading produces several key changes in the silicon parameters. First, the band gap (E_g) decreases through strain-induced band structure renormalization. The dielectric permittivity (ε) increases because larger interatomic distances enhance lattice polarizability. The lattice parameter (a) and Si–Si covalent bond length (d) also increase owing to pressure-induced local expansion of the unit cell and reduced crystal stiffness. Experimentally, the spectral linewidth (FWHM) also increases, indicating a higher dislocation density, disrupted lattice periodicity, and inelastic relaxation processes [31].

Analysis of silicon Raman spectra recorded in six regions from the periphery to the epicenter of a shock wave with an amplitude of ~ 2 GPa reveals a consistent evolution of the LO phonon position, full width at half maximum, integrated intensity, and peak area. These parameters reflect the combined influence of residual strain and defect rearrangement after brief impulsive loading followed by relaxation at room temperature. Shock loading generates defects including vacancies, interstitials, a small number of dislocation configurations, and a limited number of stacking faults [32]. Their combined effects and spatial distribution determine the observed Raman spectral changes.

We identified a key indicator of the system state: the frequency shift of the principal silicon LO mode relative to the reference value of 520.0 cm^{-1} for an unloaded crystal. The frequency was 519.24 cm^{-1} at the edge and fell to 517.88–517.92 cm^{-1} toward the center. Thus, the overall negative shift lies in the range 1.35–1.45 cm^{-1}. The equivalent residual tensile stress (~ 0.26–0.30 GPa) was calculated using the calibration coefficient $\partial\omega/\partial P \approx 5.2$ cm^{-1}/GPa. This coefficient was chosen because it originates from conventional hydrostatic experiments (0–5 GPa), traditionally forming the basis of the Varshni model for the linear pressure sensitivity of the LO phonon frequency. Since the measured strains are very small and remain within the linear response regime, using

this constant is considered the only appropriate means of verifying the stress state.

The integrated peak intensity changes more strongly than the FWHM. The decrease from its maximum toward the central regions is 65−72 %. This substantial reduction cannot be explained by elastic strain alone; it indicates a considerable decrease in the phonon coherence length caused by point defects and small dislocation configurations, which disrupt the phase coherence of lattice vibrations at the nanoscale. Whereas conventional dislocations are primarily responsible for long-lived stress fields, point defects play the dominant role in reducing phonon coherence and thus trigger the observed intensity decrease [33,34].

The linewidth increases from 6.29 to 6.78 cm^{-1}, i.e., by only 7−8 %, whereas the integrated intensity and peak area fall by more than 60 %. This combination of modest broadening and a large intensity decrease is characteristic of conditions in which the dominant increase is in the probability of phonon scattering by point defects, rather than in the nonuniformity of crystal stress, shortening the phonon coherence length. Under these conditions, the line shape remains close to the initial one, but its amplitude and area decrease sharply [35]. This behavior agrees with calculations of phonon damping dynamics in moderately defective silicon, where coherence loss dominates over inhomogeneous broadening and the dislocation contribution to FWHM is small because of the low dislocation density produced by a 2 GPa shock wave.

Combined analysis of the frequency, FWHM, intensity, and spectral peak area confirms that residual tensile stress predominates. Point defects and short dislocation configurations make the dominant contribution to Raman spectral degradation by reducing phonon coherence. Use of the calibration coefficient $\partial\omega/\partial P \approx 5.2\,cm^{-1}$/GPa is justified experimentally and methodologically, because the strain levels and defect types correspond to the regime in which the LO phonon frequency shift depends linearly on equivalent pressure. The observed spectral changes are consistent with the physical picture of the residual defect and stress structure after shock-wave passage and support the chosen approach to interpreting strain and defects from Raman spectra.

The sensitivity of the band gap and dielectric permittivity to mechanical loading can be used to develop highly sensitive strain-photonic sensors [36] based on real-time Raman monitoring of the material state. Changes in the lattice parameter and vibrational modes under impulsive waves suggest the possibility of developing shock-resistant optical waveguides and integrated optical structures with tunable dispersion. The observed trends can guide optimization of power semiconductor components, where mechanical stress critically affects service life and operational stability.

Combining the modified Varshni model with RS could provide a basis for nondestructive assessment of the service life of next-generation devices operating under extreme loads. Such approaches are particularly promising for laser processing, high-speed electronics, and photonics, where materials with predictable behavior under impulsive loading are needed.

6. Conclusion

The analysis shows that combining RS with the Varshni model provides an informative tool for diagnosing shock-induced changes in silicon. An LO phonon redshift of 1.35−1.45 cm^{-1} and a moderate linewidth increase of 7−8 % were observed experimentally. The integrated peak intensity decreased by 65−72 %, reflecting the influence of newly formed point defects. Despite the dynamic nature of the process, the property changes follow linear dependences. These results agree with model predictions of band gap narrowing, increased dielectric permittivity, and lattice expansion, demonstrating the method's potential for analyzing materials under impulsive loading and assessing semiconductor service life without destroying the sample.

Funding

This research was supported under a state assignment of the Ministry of Science and Higher Education of the Russian Federation, project FSSS-2026-0009.

Conflict of interest

The authors declare that they have no conflict of interest.

References

[1] D. Naumenko, V. Snitka, M. Duch, N. Torras, J. Esteve. Microelectron. Eng., **98**, 488 (2012). DOI: 10.1016/j.mee.2012.07.089
[2] Y. Zhang. Opt. Express, **29** (12), 18923 (2021). DOI: 10.1364/OE.427845
[3] S. Meier. *Resonant Raman spectroscopy of semiconductor structures*, Diss. (Regensburg, Univ. Regensburg, 2022).
[4] S.X. Hu, B. Militzer, L.A. Collins, K.P. Driver, J.D. Kress. Phys. Rev. B, **94**, 094109 (2016). DOI: 10.1103/PhysRevB.94.094109
[5] O. Strickson, E. Artacho. J. Phys.: Condens. Matter, **27**, 305401 (2015). DOI: 10.1088/0953-8984/27/30/305401
[6] A. Higginbotham, P.G. Stubley, A.J. Comley, J.H. Eggert, J.M. Foster, D.H. Kalantar, D. McGonegle, S. Patel, L.J. Peacock, S.D. Rothman, R.F. Smith, M.J. Suggit, J.S. Wark. Sci. Rep., **6**, 24211 (2016). DOI: 10.1038/srep24211
[7] S. Pandolfi, S.B. Brown, P.G. Stubley, A. Higginbotham, C.A. Bolme, H.J. Lee, B. Nagler, E. Galtier, R.L. Sandberg, W. Yang, W.L. Mao, J.S. Wark, A.E. Gleason. Nature Commun., **13**, 5535 (2022). DOI: 10.1038/s41467-022-33220-0
[8] S. Sun. J. Phys. D: Appl. Phys., **46**, 135301 (2013). DOI: 10.1088/0022-3727/46/13/135301
[9] S. Utamuradova. Materials Today Proceedings, **69**, 378 (2023). DOI: 10.1016/j.matpr.2023.03.456
[10] X. Wang. Progr. Mater. Sci., **125**, 100128 (2022). DOI: 10.1016/j.pmatsci.2021.100128

[11] J. Geurts. Phys. Status Solidi B, **252**, 1770 (2015). DOI: 10.1002/pssb.201552312
[12] P.K. Sarswat, S.K. Pandey. Comput. Mater. Sci., **51**, 7 (2011). DOI: 10.1016/j.commatsci.2011.05.033
[13] M. Ji, X. Guo, L. Chen. J. Appl. Phys., **122** (8), 085702 (2017). DOI: 10.1063/1.4999645
[14] R. Pässler. Phys. Status Solidi B, **248**, 1517 (2011). DOI: 10.1002/pssb.201046424
[15] K. Ghosh, A. Singha. IEEE Trans. Electron Dev., **63** (4), 1657 (2016). DOI: 10.1109/TED.2016.2529302
[16] N. Singh. Solid-State Electron., **152**, 9 (2019). DOI: 10.1016/j.sse.2018.11.004
[17] N. Ovsyuk, S. Lyapin. Appl. Phys. Lett., **116** (6), 062103 (2020). DOI: 10.1063/1.5134768
[18] S. Zhao, E.N. Hahn, B. Kad, B.A. Remington, C.E. Wehrenberg, E.M. Bringa, M.A. Meyers. Acta Mater., **103**, 519 (2016). DOI: 10.1016/j.actamat.2015.09.022
[19] M. Afshar, J. Walia, P. Berini, F. Variola, R. Bhardwaj. J. Raman Spectrosc., **51** (9), 1732 (2020). DOI: 10.1002/jrs.5932
[20] M. Bowden, D.J. Gardiner, D. Wood. J. Micromech. Microeng., **11** (1), 7 (2001). DOI: 10.1088/0960-1317/11/1/302
[21] C. Wang, G.-Y. Wang, H.-M. Zhang, J.-J. Song, C.-D. Yang, Y.-F. Mao, Y.-M. Li, H.-Y. Hu, R.-X. Xuan. Acta Phys. Sin., **61** (4), 047203 (2012). DOI: 10.7498/aps.61.047203
[22] K.-D. Liss, T. d'Almeida, M. Kaiser, R. Hock, A. Magerl, J.F. Eloy. J. Appl. Phys., **106** (4), 044914 (2009). DOI: 10.1063/1.3204968
[23] Hiroaki Kishimura, Hitoshi Matsumoto. J. Appl. Phys., **103** (2), 023505 (2008). https://doi.org/10.1063/1.2830805
[24] E. Anastassakis, A. Cantarero, M. Cardona. Phys. Rev. B, **41**, 7529 (1990). DOI: 10.1103/PhysRevB.41.7529
[25] Z. Li, P. Graziosi, N. Neophytos. Phys. Rev. B, **104**, 195201 (2021). DOI: 10.1103/PhysRevB.104.195201
[26] Y.P. Varshni. Physica, **34** (1), 149 (1967). DOI: 10.1016/0031-8914(67)90062-6
[27] G.A. Samara. Phys. Rev. B, **27**, 3494 (1983). DOI: 10.1103/PhysRevB.27.3494
[28] M. Kadlečíková, L'. Vančo, J. Breza, M. Mikolášek, K. Hušeková, K. Fröhlich, P. Procel, M. Zeman, O. Isabella. Optik, **257**, 168869 (2022). DOI: 10.1016/j.ijleo.2022.168869
[29] Y. Sano, K. Oguchi, K. Tsuji, T. Ikeuchi, M. Tagawa. Opt. Express, **33**, 41824 (2025). DOI: 10.1364/OE.571558
[30] V.V. Emtsev, V.V. Toporov, G.A. Oganesyan, A.A. Lebedev, D.S. Poloskin. Physica B, **684**, 415949 (2024). DOI: 10.1016/j.physb.2024.415949
[31] N. Roisin, M.S. Colla, J.P. Raskin, D. Flandre. J. Mater. Sci.: Mater. Electron., **34**, 373 (2023). DOI: 10.1007/s10854-022-09769-3.
[32] S. Wang, Y. Zhang. Coatings, **13**, 793 (2023). DOI: 10.3390/coatings13040793
[33] O.V. Rambadey, M. Gupta, A. Kumar, P.R. Sagdeo. J. Appl. Phys., **133**, 131101 (2023). DOI: 10.1063/5.0145442
[34] B. Liu, J. Kelsall, D.J. Ward, A.P. Jardine. Phys. Rev. Lett., **132**, 056202 (2024). DOI: 10.1103/PhysRevLett.132.056202
[35] A. Dhiman, N.S. Lewis, T. Dillard, V. Tomar. In: *Mechanical Raman Spectroscopy: Fundamentals and Applications* (Elsevier, 2021). DOI: 10.1016/B978-0-12-818278-3.00001-X
[36] C. Schriever, C. Bohley, J. Schilling, R. Wehrspohn. Materials, **5**, 889 (2012). DOI: 10.3390/ma5050889